Université Scientifique et Médicale de Grenoble

INSTITUT DES SCIENCES NUCLÉAIRES
DE GRENOBLE

53, avenue des Martyrs – GRENOBLE

ISN 84.21
March 1984

ON THE DIFFERENCE OF THE DYNAMIC MOMENT OF INERTIA $\mathcal{J}^{(2)}_{band}$ FOR Xe and Ba NUCLEI

H. EL-SAMMAN, V. BARCI, A. GIZON, J. GIZON, L. HILDINGSSON*, D. JERRESTAM*, W. KLAMRA*, R. KOSSAKOWSKI and Th. LINDBLAD*
Institut des Sciences Nucléaires, Grenoble, France

T. BENGTSSON
Department of Mathematical Physics, Lund Institute of Technology, Lund, Sweden

G.A. LEANDER
UNISOR, Oak Ridge Associated Universities, Oak Ridge, TN, U.S.A.

Permanent address : Research Institue of Physics, S 10405 Stockholm, Sweden

To appear in "Nuclear Physics A".

Laboratoire associé à l'Institut National de Physique Nucléaire et de Physique des Particules.

ON THE DIFFERENCE OF THE DYNAMIC MOMENT OF INERTIA $\mathcal{J}^{(2)}_{band}$ FOR Xe and Ba NUCLEI

H. EL-SAMMAN, V. BARCI, A. GIZON, J. GIZON, L. HILDINGSSON,[†]
D. JERRESTAM[†], W. KLAMRA[†], R. KOSSAKOWSKI and Th. LINDBLAD[†].

Institut des Sciences Nucléaires (IN2P3, USMG)
53 Avenue des Martyrs
38026 - Grenoble Cédex (France)

T. BENGTSSON
Department of Mathematical Physics
Lund Institute of Technology
S - 22007 Lund, Sweden

and

G.A. LEANDER
UNISOR, Oak Ridge Associated Universities
Oak Ridge, Tennessee, USA

[†] Permanent address : Research Institute of Physics, S 10405, Stockholm, Sweden

Abstract : The γ-rays following the $^{112,117,122}Sn + ^{12}C$ and $^{123}Sb + ^{12}C$ reactions have been investigated using six NaI(Tl) detectors in a two-dimensional arrangement. The γ-ray multiplicities have been measured and the dynamic moments of inertia $\mathcal{J}^{(2)}_{band}$ of $^{118,122}Xe$ and $^{128,130}Ba$ extracted from the energy-correlation spectra. The behaviour of these nuclei and the observed difference of $\mathcal{J}^{(2)}_{band}$ in Xe and Ba nuclei are interpreted in terms of high-spin collective properties.

E

NUCLEAR REACTIONS $^{112,117,122}Sn + ^{12}C$, E = 80 - 118 MeV ; $^{123}Sb + ^{12}C$, E = 118 MeV ; measured γγ-coin, γ-ray multiplicity ; deduced γγ-energy correlation matrices and dynamic moment of inertia $\mathcal{J}^{(2)}_{band}$.

1. Introduction

The investigation of high-spin states in rotational nuclei can be performed by studying the discrete γ-rays depopulating such levels. High resolution Ge detectors in conjunction with e.g. BGO anti-Compton shields has recently turned out to be a very powerful tool [1].

Another method involves the study of the apparent continuum using NaI(Tl) detectors which have poorer energy-resolution but higher photopeak efficiencies. A singles spectrum recorded with such a detector will only show a few of the most intense transitions. However, for a rotational nucleus, the spectrum will exhibit a low energy ($E_\gamma \lesssim 2$ MeV) bump consisting of mainly E2 transitions reflecting the rotational character of the nucleus and a high energy exponential tail involving the statistical transitions. Although the E2 bump may not be resolved into individual transitions, several interesting properties can be obtained. Thus, the sum-spectrometer and γγ-energy correlation techniques can be applied in order to yield informations on the moment of inertia [2,3].

During the last few years several experiments have been performed in the Ba-Xe region [cf ref. 4,5 and the pertinent references therein]. These investigations have revealed different behaviour of the dynamic moment of inertia with the rotational frequency. In order to gain further knowledge on this behaviour, experiments were undertaken at the Grenoble cyclotron to study light Xe nuclei and the heavier Ba nuclei.

2. Experimental techniques

Six NaI(Tl) detectors are used to record γγ-coincidence spectra. They are 8" long and have a hexagonal cross-section with a 6" outer diameter.

To prevent scattering, they are shielded with lead and their entrance window is collimated. They are placed at 25 cm from the target at an angle of 125° relative to the beam. Their solid angle is 0.27 % of 4π and their energy resolution is better than 8 % for the 661 keV γ-line of ^{137}Cs.

In order to identify the final reaction products, the experiment also involves a high resolution Ge detector. This detector has an efficiency of 40 % and an energy resolution of 1.9 keV at 1332 keV and is positioned perpendicular to the beam axis. An example of a spectrum recorded with the Ge counter is shown in fig. 1.

Four enriched self-supporting targets of about 4 mg/cm^2 thickness are bombarded with ^{12}C ions from the Grenoble variable energy cyclotron. Further details on the experimental conditions are given in table 1 where the identified final nuclei are listed with their relative intensities deduced from prompt in-beam γ-ray spectra of the Ge detector in coincidence with two or more NaI(Tl) crystals.

For each of the targets, approximately 70×10^6 NaI(Tl) coincidence events are recorded. This is achieved with a beam current of $\sim$ 1 pnA, which yields, on the average, a coincidence counting rate of 1500 cps. Since all events involving two or more detectors in coincidence are written on magnetic tapes to be subsequently analyzed into one single matrix, the gains of the amplifiers are carefully matched and monitored throughout the experiment.

In a separate experiment, the γ-ray multiplicities are determined for the ^{112}Sn and ^{122}Sn targets. They are deduced from the number of counters (12 NaI(Tl) crystals of a sum spectrometer) triggered in coincidence with a Ge detector. Examples of fold-distributions relative to the ground state transitions in $^{128,130}Ba$ obtained in the $^{122}Sn + {}^{12}C$ reaction are shown in fig. 2.

3. Experimental results

As in previous measurements, the coincidence data are sorted off-line into a two-dimensional matrix. In order to improve the apparent statistics, this matrix is made symmetric with respect to $E_\gamma^{(1)} = E_\gamma^{(2)}$. Since most of the coincidence events are not correlated photopeak-photopeak events, the Copenhagen subtraction scheme [3] is applied in order to enhance the correlated ones.

This matrix of correlated events obtained in this manner will exhibit several features. Thus for a perfect rotor having level energies proportional to $I(I+1)$, the transition energies ($\Delta I = 2$)

$$E_\gamma = \frac{\hbar^2}{2\mathcal{J}} \quad (4\,I-2)$$

will generate a pattern with no intensity along the diagonal $E_\gamma^{(1)} = E_\gamma^{(2)}$ with adjacent ridges at distances ΔE_γ from this diagonal. In other words, the width of the valley W measures twice the difference in transition energies, i.e.

$$W = 2\,\Delta E_\gamma = 4\,\frac{dE_\gamma}{dI} = 8\,\frac{d^2E}{dI^2} \equiv 16\,\frac{\hbar^2}{2\mathcal{J}^{(2)}_{band}}$$

where E is the excitation energy and $\mathcal{J}^{(2)}_{band}$ is a dynamical moment of inertia.

For real nuclei, $\mathcal{J}^{(2)}_{band}$ will not be constant. The variations of this moment of inertia with rotational frequency, $\hbar\omega = E_\gamma/2$ can be obtained from the width of the valley. In the present experiment we deduce $\mathcal{J}^{(2)}_{band}$ from the width of the valley in the correlation matrix by measuring the distance between the tops of the peaks of the first ridge in cuts perpendicular to the diagonal. Depending on the nucleus and on the statistics, these cuts are made 15,30 or 45 keV wide. The error bars are due to the statistics and to the existence of composite peaks.

Other interesting features in a correlation matrix are the appearance of "bridges" accross the valley and "stripes" parallel to the energy axes. Such features are typical of the backbending phenomenon and will provide us with informations on band crossings and rotational alignment of particles of high j orbitals whose frequencies can be compared with model calculations. These features appear in the correlation matrices shown in figs. 3, 4, 5, 6.

3.1. The ^{112}Sn + ^{12}C reaction at 112 MeV

The main final nuclei obtained when bombarding the ^{112}Sn target with 112 MeV ^{12}C-ions are ^{118}Xe and ^{116}Te. This feature is evident from fig. 1 and table 1.

In this experiment, the γ-multiplicities were measured. Most of the γ-lines of ^{116}Te are not well separated in the spectra which explains why the results do not show a significant difference between ^{118}Xe and ^{116}Te, though one would expect the ^{116}Te nucleus to have a smaller value since it is formed following the emission of two more protons. This argument together with the relative intensities implies that the energy-energy correlation matrix (fig.3) in the ^{112}Sn + ^{12}C reaction is dominated by ^{118}Xe at high γ-ray energies.

This matrix does not exhibit a well defined valley at lower energies. Furthermore, when the valley starts to develop at E_γ = 0.450 MeV, it is a valley with many "fillings" and bridges. This explains why there are only a few values of $\mathcal{J}^{(2)}_{band}$ determined up to $\hbar^2\omega^2$ = 0.08 MeV^2 (fig. 7). The strong bridge at E_γ = 0.775 MeV is due to the irregularities in the rotational structure of the ^{118}Xe ground band at $I^\pi = 8^+ - 18^+$, i.e. the first backbend. The highest value (44 $\hbar^2$ MeV^{-1}) of $\mathcal{J}^{(2)}_{\rm band}$ results in the narrowing of the valley due to the coincidence between the 0.742 and 0.676 MeV γ-rays deexciting the 12^+ and 8^+ levels in ^{118}Xe, respectively. The final nucleus ^{116}Te contributes to the low-energy part of the correlation matrix and produces a bridge at $E_\gamma = 0.67$ MeV.

For frequencies higher than $\hbar^2\omega^2 = 0.17$ MeV^2, the moment of inertia $\mathcal{J}^{(2)}_{\rm band}$ is almost constant and equals 30 $\hbar^2$ MeV^{-1} on both side of a filling in the valley at $E_\gamma = 1.01$ MeV ($\hbar^2\omega^2 = 0.254$ MeV^2). Our data end on a strong bridge at $E_\gamma = 1.20$ MeV.

3.2 <u>The ^{117}Sn + ^{12}C reaction at 118 MeV</u>

The nuclei ^{123}Cs, $^{120-123}$Xe and ^{118,121}Te are clearly identified in the singles and coincidences germanium spectra. From the ratios of γ-rays intensities in the spectrum of a Ge detector in coincidence with two or more NaI crystals to the singles, it appears that the xenons and ^{123}Cs have approximately the same multiplicity which is much larger than that of the telluriums, as expected. Such a ratio is not enough precise to make a difference between the xenons and cesium but considering the intensities in the various channels ^{122}Xe dominates very likely in the high energy part of the correlation matrix (fig.4).

The main bridge at $E_\gamma = 0.79$ MeV corresponds to the backbend in ^{122}Xe and ^{120}Xe. The dynamic moment of inertia $\mathcal{J}^{(2)}_{\rm band}$ (fig. 8) which is equal to 34 $\hbar^2$ MeV^{-1} at the maximum drops down to 25 $\hbar^2$ MeV^{-1} after the first backbend and remains almost constant up to $\hbar^2\omega^2 = 0.46$ MeV^2. This last point is equivalent to a 1.35 MeV γ-ray energy.

3.3 The $^{122}Sn + ^{12}C$ reaction at 80 MeV

Only neutrons are emitted in this reaction which occurs at lower energy on a heavier target. ^{128}Ba is produced with the lowest percentage (table 1) and ^{129}Ba is obtained in a large quantity which is shared by the $h_{11/2}$ and $g_{7/2}$ bands [6], each being made of two main cascades.

The γ-rays belonging to the three different nuclei are well separated in the γ-spectra. This gives unambiguous results concerning our γ-multiplicity measurements. It clearly appears in fig. 2 and table 1 that the ^{130}Ba γ-lines are associated with the largest prompt multiplicity ($< M_\gamma > \simeq 15$) to be compared with the ^{129}Ba ($< M_\gamma > \simeq 13$) and ^{128}Ba ($< M_\gamma > \simeq 12$) cases. In conclusion, $^{129,130}Ba$ are the preponderant nuclei in the correlation matrix (fig.5).

A very clear valley appears in the matrix up to 1.14 MeV γ-ray energy whose width decreases continuously. There is no apparent bridge between E_γ = 0.400 and 1.095 MeV. However a hill in the botton shows up very clearly at E_γ = 0.760 MeV in a cut made along the first diagonal. It results in coincidences between the 0.794 and 0.729 MeV γ-lines depopulating the 14^+ and 12^+ levels in the backbending region of ^{130}Ba.

It may be noted in fig. 9 that after this backbend, $\mathcal{J}^{(2)}_{band}$ increases very slightly up to approximately 90 % of the rigid rotor value (46 $\hbar^2$ MeV^{-1}) near the strong bridge which terminates the valley at E_γ = 1.095 MeV. Then, $\mathcal{J}^{(2)}_{band}$ possibly increases to this value at $\hbar^2\omega^2 \gtrsim 0.33$ MeV^2 i.e. a rotational frequency $\hbar\omega$ = 0.57 MeV.

3.4 The $^{123}Sb + ^{12}C$ reaction at 118 MeV

The same kind of analysis can be made for the ^{123}Sb target experiment. ^{129}La could have a very slightly larger angular momentum than ^{128}Ba since it is produced in the (^{12}C,6n) reaction to be compared with the (^{12}C,p6n) channel, but ^{128}Ba represents 46 % of the total activity i.e. three times more than ^{129}La. Considering this preponderant percentage, it appears that ^{128}Ba should be the nucleus which mainly influences the energy-energy correlation matrix (fig. 6).

The variations of $\mathcal{J}^{(2)}_{band}$ in function of $\hbar^2\omega^2$ are plotted in the range 0.07 - 0.36 MeV^2 (fig. 10). The bridge at E_γ = 0.890 MeV corresponds exactly to the coincidence between the lines deexciting the 12^+ and 10^+ levels in ^{128}Ba. When going to higher frequencies, $\mathcal{J}^{(2)}_{band}$ increases up to the rigid body value (45 $\hbar^2$ MeV^{-1}) at $\hbar^2\omega^2$ = 0.32 MeV^2 and could reach 50 $\hbar^2$ MeV^{-1} near $\hbar^2\omega^2$ = 0.36 MeV. One must point out the existence of a bridge at 1.040 MeV and the very low value (32.5 $\hbar^2$ MeV^{-1}) at $\hbar^2\omega^2$ = 0.255 MeV^2 which constitutes a dip in the $\mathcal{J}^{(2)}_{band}$ curve.

4. Discussion of the dynamic moment of inertia $\mathcal{J}^{(2)}_{band}$

The collective moment of inertia of the ground band which is related to the discrete γ transitions by the formula $\mathcal{J}^{(1)} \equiv \frac{\hbar}{4} \times \frac{4I-2}{\omega}$ can be parametrized within the VMI model i.e.

$$\mathcal{J}^{(1)}_{yrast}\ (\omega) = \hbar\ \frac{I}{\omega} = \mathcal{J}_0 + \mathcal{J}_1\omega^2 \qquad (1)$$

where $\mathcal{J}_0$ and $\mathcal{J}_1$ are two parameters.

The dynamic moment of inertia $\mathcal{J}^{(2)}_{band}$ which is deduced from the width of the valley in a correlation matrix and is proportional to the first derivative $\frac{dI}{d\omega}$ can be compared to $\mathcal{J}^{(2)}_{yrast} = \mathcal{J}_0 + 3\,\mathcal{J}_1\omega^2$ obtained by differenciation of equation (1). In this development, the alignment of particles which takes place at the backbend has not been considered since the aligned angular momentum i is constant inside a band.

4.1 The xenon nuclei

As a general remark, one sees from the $\mathcal{J}^{(2)}_{band}(\omega^2)$ curves that both the above defined moments of inertia $\mathcal{J}^{(2)}_{band}$ and $\mathcal{J}^{(2)}_{yrast}$ agree well up to the frequencies of the first backbend. This is valid up to $\hbar^2\omega^2 = 0.08$ MeV^2 for ^{118}Xe.

In fig. 6, one notices that the measured values of $\mathcal{J}^{(2)}_{band}$ are separated in two sets, both fitting the straight lines $\mathcal{J}_0 + 3\mathcal{J}_1\omega^2$ corresponding to ^{120}Xe and ^{122}Xe. This is explained by the strong discrete lines deexciting the first levels of these two nuclei which are well defined in the low energy region of the correlation matrix.

$\mathcal{J}^{(2)}_{band}$ of both ^{118,122}Xe behave in a similar way i.e. decrease strongly after the first backbend down to roughly two thirds of the rigid sphere value (figs. 5 and 6). This first backbending in ^{124,126,128,130}Xe originates from the coupling of two $h_{11/2}$ neutrons [7] but, up to now, there is no definite answer for it in the lighter xenon isotopes. However, calculations made in the Bengtsson and Frauendorf model [8] indicate that band crossings of $h_{11/2}$ protons and neutrons can occur at nearby frequencies, the latter being more probable.

Our data on ^{118}Xe enlarge towards lighter masses and more neutron-deficient nuclei previous measurements made on xenon isotopes [4,5]. Our results on ^{122}Xe extend to higher frequencies (up to $\hbar\omega = 0.67$ MeV) the data already known from the ^{116}Sn + ^{12}C reaction [4].

4.2 The barium nuclei

As in the xenons, the experimental $\mathcal{J}^{(2)}_{band}$ values, can be fitted with a $\mathcal{J}_0 + 3\mathcal{J}_1\omega^2$ polynomial below the first particle alignment.

The variations of $\mathcal{J}^{(2)}_{band}$ in both $^{128,130}Ba$ look very similar (figs. 9 and 10) except for the reduction in ^{128}Ba at $\hbar^2\omega^2 = 0.255$ MeV^2 immediately after the backbend. This reduction is less pronounced than in ^{126}Ba where it produces a deep minimum also centered around $\hbar^2\omega^2 = 0.25$ MeV^2, [ref. 4]. We show in fig. 9, that this dip has disappeared in ^{130}Ba or almost entirely disappeared if one takes into account the very shallow minimum at $\hbar^2\omega^2 = 0.185$ MeV^2. This could mean that the collective moment of inertia is less affected by particle alignment in ^{130}Ba than in $^{126,128}Ba$. According to the intuitive picture of Deleplanque et al. [9] this would be connected with the fact that the aligned angular momentum above the first band crossing in ^{130}Ba [ref. 10] is smaller by roughly two units than in the ^{126}Ba and ^{128}Ba cases [11,12].

Two band crossings have been found in ^{128}Ba, [ref. 11] and ^{130}Ba [ref. 10] Alignment considerations and cranking model calculations agree to predict a $h_{11/2}$ neutron origin for the lowest one in ^{130}Ba while the second is generated by $h_{11/2}$ protons [10], the backbend in ^{126}Ba having also a $h_{11/2}$ proton nature. A backbend has been found in ^{130}Ce, [ref. 1] at high frequency ($\hbar\omega = 0.58$ MeV). This third one (after the $\pi h_{11/2}$ and $\nu h_{11/2}$ alignments) is expected from $i_{13/2}$ neutrons. If the isotones behave the same way, ^{128}Ba should also exhibit such a high frequency alignment. We propose that the bridge observed at $\hbar\omega = 0.52$ MeV in the ^{128}Ba correlation matrix could proceed from $i_{13/2}$ neutrons as the one found at $\hbar\omega = 0.55$ MeV in ^{130}Ba.

4.3. The difference observed between the Ba and Xe nuclei

A major difference appears when comparing the xenons and the bariums : the moment of inertia of the former decreases after the first band crossing and remains small and almost constant at high frequency while it increases in the latter all along with the frequency. Such a qualitative difference in the quasicontinuum data could reflect changes in the high-spin collective properties, particularly the shape, with changing nucleon number. Both the proton and neutron numbers are larger in the barium than the xenon isotopes we have studied.

For a possible interpretation of the results we can look to high-spin potential energy of deformation surfaces, which have been calculated for these nuclei by the cranked Nilsson-Strutinsky method [13]. A recent study [14] which also included pairing has clarified systematic trends of microscopic origin which are manifested by the numerical results : the alignment of high-j quasiparticle orbitals drives the nuclear shape toward regions of collective or non-collective rotation, depending on the position of the Fermi levels in the j-shell. The valence shells of light xenon and barium isotopes include the neutron and proton $h_{11/2}$ intruder shells. The general systematics of reference 14 would suggest a more collective behaviour in the bariums than the xenons after initial quasiparticle alignment, considering the position of the Fermi level in these shells. We have carried out calculations using the method of reference 15 where individual bands are constructed and traced up to high spins. Table 2 and figures 11 and 12 show the results for the nuclei ^{122}Xe and ^{128}Ba, which we have chosen for a closer theoretical study. From a study of the potential energy surfaces of reference 13, it follows that the differences between ^{130}Ba and ^{128}Ba are rather small and ^{118}Xe is similar to ^{122}Xe except that it tends to be a little more collective.

In ^{122}Xe, we find three different kinds of states near yrast (c.f. table 2 and fig. 11). There are collective prolate bands at $\gamma \approx 0$ with $\mathcal{J}^{(2)}_{\mathrm{band}} \gtrsim 35\ \hbar^2\ \mathrm{MeV}^{-1}$;

moderately collective triaxial bands at $\gamma \approx 30°$ with $\mathcal{J}^{(2)}_{\text{band}} < 30\,\hbar^2\,\text{MeV}^{-1}$, and non-collective states of particle-hole character at $\gamma = 60°$. The data can be taken to indicate that it is the $\gamma \approx 30°$ triaxial bands which come lowest in energy and dominate the γ cascade in ^{122}Xe. Actually, the non-collective states come lower in the present calculation (fig. 11), but the precise relative position of such different classes of states is highly sensitive to the single-particle parameters of the model, and is not as reliably predicted as the characteristic properties within each class of states. If the non-collective states are only near yrast, they need not be evidenced by the present experiment which selectively brings out collective features. The observed features in ^{122}Xe fit the description of the moderately collective, $\gamma \approx 30°$ triaxial bands.

For ^{128}Ba, the calculated near-yrast levels are collective with $\mathcal{J}^{(2)}_{\text{band}} > 30\,\hbar^2\,\text{MeV}^{-1}$. A further mechanism for the continued increase of $\mathcal{J}^{(2)}_{\text{band}}$ at high spins in ^{128,130}Ba, but not ^{118,122}Xe, is provided by a secondary minimum at larger deformation in the potential-energy surfaces [13]. This minimum at $\varepsilon \sim 0.34$, $\gamma \sim 0°$ corresponds to bands with a pair of aligned $h_{9/2}$ neutrons. With additional $i_{13/2}$ neutron alignment such bands may cross the valence bands and become yrast at very high spins [16]. The energy of the strongly deformed ($\varepsilon \sim 0.34$) potential-energy minimum relative to the valence-shell ($\varepsilon \sim 0.24$) minimum decreases for increasing proton and neutron number up to an optimum of about $Z = 60$ and $N = 72$, [ref. 13]. For the barium isotopes ($Z = 56$, $N = 72, 74$) these bands are not expected to be yrast at the very highest spins reached in the present experiment. Nevertheless, over a wide range of lower spins they are likely to retain a significant fraction of the total population from a (HI, yPxn) reaction (fig. 12). These strongly collective bands would then dominate the $E_\gamma - E_\gamma$ correlations and account for the larger $\mathcal{J}^{(2)}_{\text{band}}$ values in the barium isotopes. Calculated $\mathcal{J}^{(2)}_{\text{band}}$ values for a few configurations are given in table 2.

The interpretation of the data suggested above could be tested by extending the experimental systematics to light Ce, Nd and Sm nuclei.

Acknowledgements

We thank Prof. Z. Szymanski and Dr. S. Åberg for very fruitful discussions. We are indebted to the cyclotron crew for providing the beams and to Mr. G. Margotton for technical assistance. This work was supported in part by Centre National de la Recherche Scientifique, by the Swedish Research Council for Natural Sciences (U-FR-8219-114) and by UNISOR,a consortium of 12 institutions, supported by them and by the Office of Energy Research of the U.S.D.O.E. under contract DE-AC05-76OR00033 with Oak Ridge Associated Universities.

References

1) P.J. Nolan, R. Aryaeinejad, A.H. Nelson, D.J.G. Love, D.M. Todd and P.J. Twin, Proc. Int. Conf. on Nuclear Physics, Florence, (1983), p. 149 and Phys. Lett. 128B (1983) 285

2) H.J. Körner, D.L. Hillis, C.P. Roulet, P. Aguer, C. Ellegaard, D.B. Fossan, D. Habs, M. Neiman, R.S. Stephens and R.M. Diamond, Phys. Rev. Lett., 43 (1979) 490

3) O. Anderson, J.D. Garrett, G.B. Hagemann, B. Herskind, J.L. Hillis and L.L. Riedinger, Phys. Rev. Lett., 43 (1979) 687

4) Th. Lindblad, L. Hildingsson, D. Jerrestam, A. Källberg, A. Johnson, C.J. Herrlander, W. Klamra, A. Kerek, C.G. Linden, J. Kownacki, J. Bialkowski and T. Vertse, Nucl. Phys., A378 (1982) 364

5) W. Klamra, J. Bialkowski, C.J. Herrlander, L. Hildingsson, D. Jerrestam, A. Johnson, A. Kerek, J. Kownacki, A. Källberg, Th. Lindblad, C.G. Linden, and T. Vertse, Nucl. Phys., A391 (1982) 184

6) J. Gizon, A. Gizon and J. Meyer-ter-Vehn, Nucl. Phys. A277 (1977) 464

7) H. Hanewinkel, W. Gast, U. Kaup, H. Harter, A. Dewald, A. Gelberg, R. Reinhardt, P. Von Brentano, A. Zemel, C.E. Alonso and J.M. Arias, Phys. Lett., 133B (1983) 9

8) R. Bengtsson and S. Frauendorf,
Nucl. Phys., A327 (1979) 139

9) M.A. Deleplanque, F.S. Stephens, O. Andersen, J.D. Garrett, B. Herskind, R.M. Diamond, C. Ellegaard, D.B. Fossan, D.L. Hillis, H. Kluge, M. Neiman, C.P. Roulet, S. Shih. and R.S. Simon,
Phys. Rev. Lett. 45 (1980) 172.

10) Sun Xiangfu, D. Bazzacco, W. Gast, A. Gelberg, U. Kamp, A. Dewald, K.O. Zell and P. Von Brentano,
Phys. Rev.. C28 (1983) 1167

11) K. Schiffer, A. Dewald, A. Gelberg, R. Reinhardt, K.O. Zell, P. Von Brentano and Sun Xiangfu,
Z. Phys. A313 (1983) 245

12) L. Hildingsson, Ph. Hubert, A. Johnson, W. Klamra and Th. Lindblad,
Phys. Scripta, 29 (1984) 45

13) S. Åberg,
Phys. Scripta, 25 (1982) 23

14) G.A. Leander, F. May and S. Frauendorf,
in 'High Angular Momentum Properties of Nuclei', ed. N.R. Johnson (Harwood, New York, 1983) p. 281

15) T. Bengtsson and I. Ragnarsson,
Phys. Lett, 115B (1982) 431

16) G.A. Leander, P. Arve, T. Bengtsson, I. Ragnarsson and J.Y. Zhang,
Nucl. Phys., A400 (1983) 970

Table captions

Table 1

Information on the reactions used in the present experiment including yields of final nuclei and multiplicities.

Table 2

Moment of inertia $\mathcal{J}^{(2)}_{band}$, for calculated bands in ^{122}Xe and ^{128}Ba. The first column shows the most important part of the configuration, then a typical deformation for this band is given, the range of spin and rotational frequency values in which the band is closest to the yrast line and has the moment of inertia given by the last column. Letters (A)-(E) refer to the curves shown in figs. 11 and 12.

Table 1

$^{112}Sn + 112$ MeV ^{12}C (80 %)[a]			$^{117}Sn + 118$ MeV ^{12}C (89 %)[a]		$^{122}Sn + 80$ MeV ^{12}C (93 %)[a]			$^{123}Sb + 118$ MeV ^{12}C (99 %)[a]	
^{117}Xe	6[b]		^{125}Cs	55[b]	^{128}Ba	18[b]	<12.0>[c]	^{127}La	27[b]
^{118}Xe	100	<14.5>[c]	^{120}Xe	65	^{129}Ba	100	<13.3>	^{129}La	37
^{119}Xe	46	<14>	^{121}Xe	80	^{130}Ba	48	<14.7>	^{128}Ba	100
^{120}Xe	9		^{122}Xe	100				^{125}Cs	54
^{116}Te	74	<14.0>	^{123}Xe	75					
^{118}Te	28	<10.7>	^{118}Te	34					
			^{120}Te	69					

a) Target enrichment.

b) Relative intensities of the ground state transition.

c) Mean multiplicity of the ground state transition.

Table 2

^{122}Xe Configuration	ε	γ	range I	range $\hbar\omega$ (MeV)	$\mathcal{J}^{(2)}_{band}$ $\hbar^2 MeV^{-1}$
$\pi(h_{11/2})^1\nu(h_{11/2})^6$	0.28	0°	6-24	-0.5	∿ 36 (A)
$\pi(h_{11/2})^1\nu(h_{11/2})^6$	0.24	33°	6-20	-0.5	∿ 28 (B)
$\pi(h_{11/2})^2\nu(h_{11/2})^6$	0.28	0°	10-36	0.1-0.7	∿ 38 (C)
$\pi(h_{11/2})^2\nu(h_{11/2})^6$	0.25	33°	18-26	0.3-0.5	∿ 30 (D)

^{128}Ba Configuration	ε	γ	range I	range $\hbar\omega$ (MeV)	$\mathcal{J}^{(2)}_{band}$ $\hbar^2 MeV^{-1}$
$\pi(h_{11/2})^2\nu(h_{11/2})^8$	0.24	-50°	4-30	-0.6	∿ 34 (A)
$\pi(h_{11/2})^2\nu(h_{11/2})^8$	0.18	5°	24-38	0.5-0.8	∿ 34 (B)
$\pi(h_{11/2})^2\nu(h_{9/2})^2$	0.34	0°	16-36	0.2-0.8	∿ 35 (C)
$\pi(h_{11/2})^3\nu(h_{9/2})^2$	0.34	0°	22-44	0.4-1.0	∿ 38 (D)
$\pi(h_{11/2})^3\nu[(h_{9/2})^2 i_{13/2}]$	0.34	0°	30-	0.4-	∿ 40 (E)

Figure captions

Fig. 1

Spectrum of γ-rays recorded with the Ge detector during the bombardment of a ^{112}Sn target with 112 MeV ^{12}C-ions. This spectrum, where the lines of ^{118}Xe are identified, is obtained in coincidence with $\geqslant$ 2 NaI(Tl) detectors and gated by the RF to produce a prompt spectrum. Cf. the text and table 1.

Fig. 2

Examples of fold-distributions used to extract the γ-ray multiplicities. The distributions are obtained by setting gates on the ground-state transitions in ^{128,130}Ba. The numbers given are the number k $\geqslant$ 5 of NaI(Tl) detectors fired in coincidence with the Ge spectrometer.

Fig. 3

Gamma-gamma energy correlation spectrum obtained from the coincidence matrix in the reaction ^{112}Sn + ^{12}C at 112 MeV.

Fig. 4

Same as fig. 3 except that the reaction here is ^{117}Sn + ^{12}C at 118 MeV.

Fig. 5

Same as fig. 3 except that the reaction here is ^{122}Sn + ^{12}C at 80 MeV.

Fig. 6

Same as fig. 3 except that the reaction here is ^{123}Sb + ^{12}C at 118 MeV.

Fig. 7

The moments of inertia $\mathcal{J}^{(1)}_{yrast}$ and $\mathcal{J}^{(2)}_{band}$ as obtained from the discrete transitions and the correlation experiment respectively (cf. the text). The solid line in the lower part of the figure is the moment of inertia $\mathcal{J}^{(2)}_{yrast}$ deduced from the lowest discrete lines. The triangles represent fillings in or bridges accross the valley. The case shown here is obtained for the ^{112}Sn target bombarded with 112 MeV ^{12}C-ions.

Fig. 8

Same as fig. 7 except that the target here is ^{117}Sn and the beam energy 118 MeV.

Fig. 9

Same as fig. 7 but obtained for the case of 80 MeV ^{12}C on ^{122}Sn.

Fig. 10

Same as fig. 7 but obtained for the case of 118 MeV ^{12}C on ^{121}Sb.

Fig. 11

Energy versus angular momentum calculated by microscopic theory for bands of ^{122}Xe. An average liquid drop contribution of 0.01I(I+1) MeV has been subtracted. Dots indicate the position of yrast non-collective states, whereas the lines indicate the bands listed in table 2. The triaxial bands are found to have almost the same energy as the prolate bands and a $\mathcal{J}^{(2)}_{band} < 30\ \hbar^2/MeV$ which is apparent as a larger curvature. With a slightly different single-particle potential the triaxial bands could well be yrast. $\mathcal{J}^{(2)}_{band}$ would not be affected by this change.

Fig. 12

Energy versus angular momentum as in fig. 11, for bands in ^{128}Ba, which suggests likely cascade and feeding patterns following a heavy-ion reaction. Labels A-E identify the same bands as in table 2. At high spins, highly collective bands like E are most probably populated. Cascades could proceed along such bands well below the spin where E crosses the yrast line, contributing strongly to the $E_\gamma - E_\gamma$ correlations. The fact that discrete transitions are hard to resolve experimentally for I > 20 can be explained partly by this mechanism, partly by the high level density in the near yrast region at I < 30 and partly by the occurence of additional, less collective, states which are obtained as yrast in this spin region.

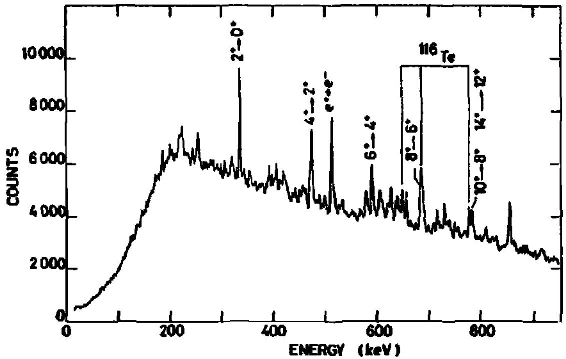

Fig. 1

Spectrum of γ-rays recorded with the Ge detector during the bombardment of a ^{112}Sn target with 112 MeV ^{12}C-ions. This spectrum, where the lines of ^{118}Xe are identified, is obtained in coincidence with ⩾ 2 NaI(Tl) detectors and gated by the RF to produce a prompt spectrum. Cf. the text and table 1.

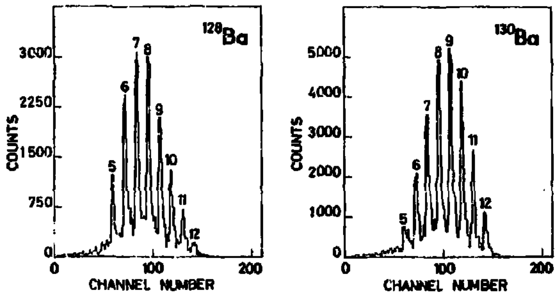

Fig. 2

Examples of fold-distributions used to extract the γ-ray multiplicities. The distributions are obtained by setting gates on the ground-state transitions in ^{128,130}Ba. The numbers given are the number $k \geqslant 5$ of NaI(Tl) detectors fired in coincidence with the Ge spectrometer.

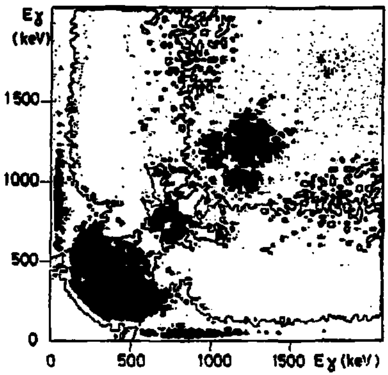

Fig. 3

Gamma-gamma energy correlation spectrum obtained from the coincidence matrix in the reaction $^{112}Sn + ^{12}C$ at 112 MeV.

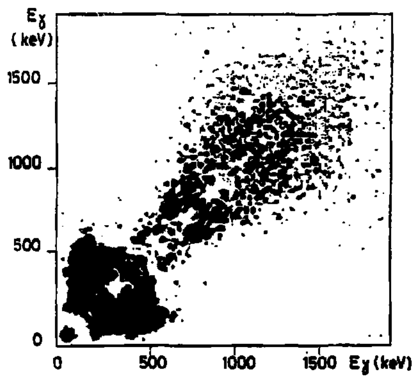

Fig. 4

Same as fig. 3 except that the reaction here is $^{117}Sn + ^{12}C$ at 118 MeV.

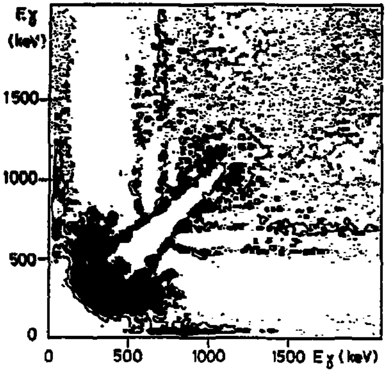

Fig. 5
Same as fig. 3 except that the reaction here is $^{122}Sn + ^{12}C$ at 80 MeV.

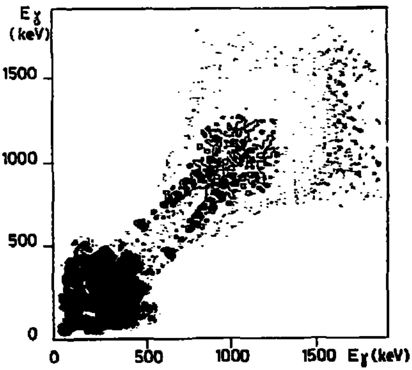

Fig. 6
Same as fig. 3 except that the reaction here is $^{123}Sb + ^{12}C$ at 118 MeV.

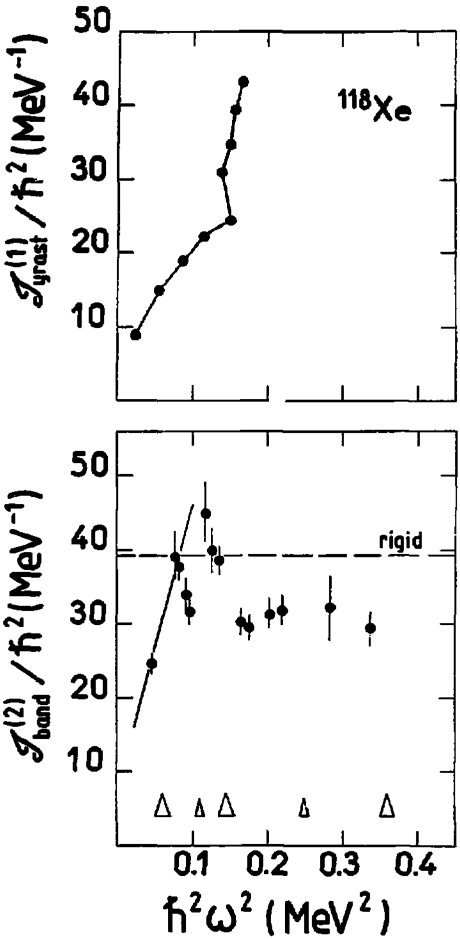

Fig. 7

The moments of inertia $\mathcal{J}^{(1)}_{yrast}$ and $\mathcal{J}^{(2)}_{band}$ as obtained from the discrete transitions and the correlation experiment respectively (cf. the text). The solid line in the lower part of the figure is the moment of inertia $\mathcal{J}^{(2)}_{yrast}$ deduced from the lowest discrete lines. The triangles represent fillings in or bridges accross the valley. The case shown here is obtained for the ^{112}Sn target bombarded with 112 MeV ^{12}C-ions.

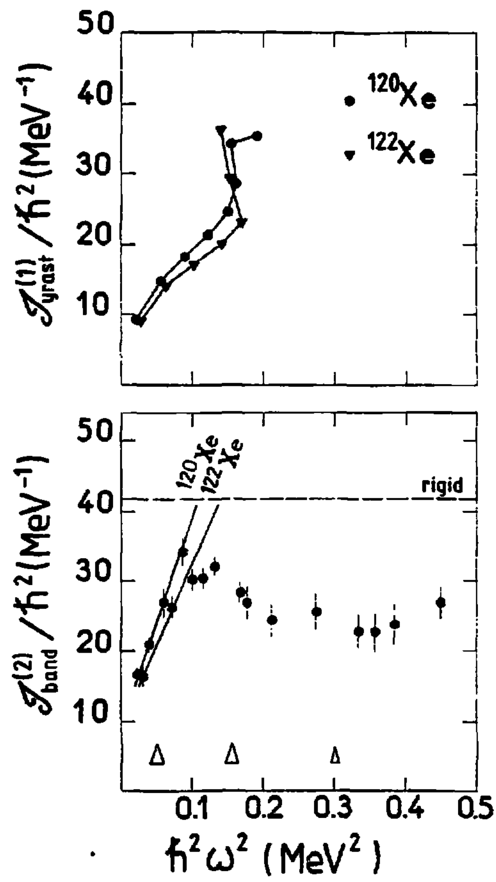

Fig. 8

Same as fig. 7 except that the target here is ^{117}Sn and the beam energy 118 MeV.

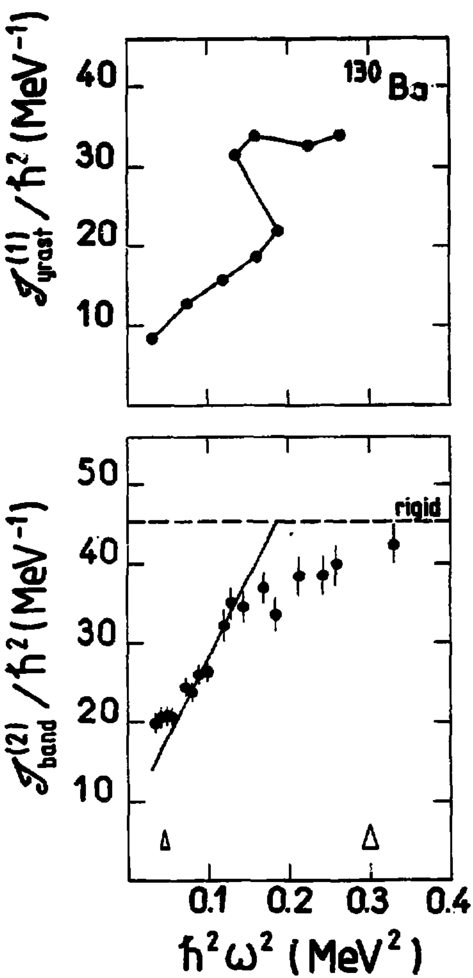

Fig. 9

Same as fig. 7 but obtained for the case of 80 MeV ^{12}C on ^{122}Sn.

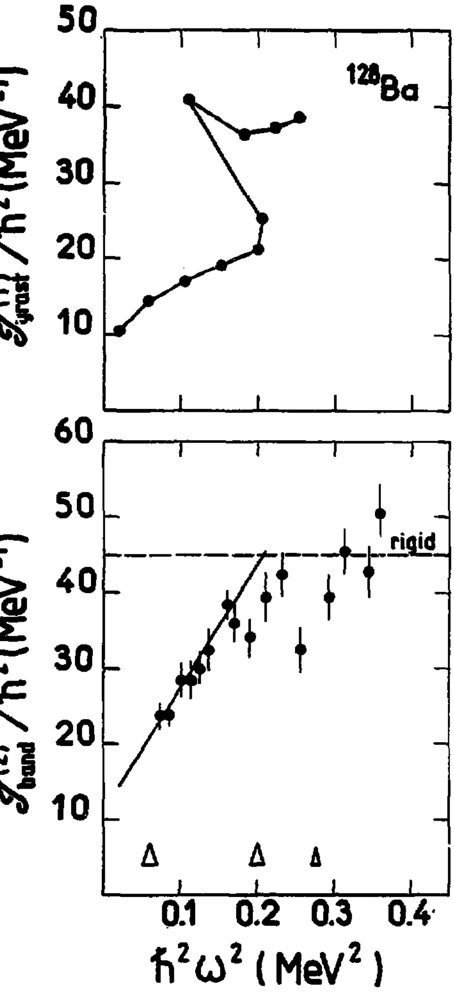

Fig. 10
Same as fig. 7 but obtained for the case of 118 MeV ^{12}C on ^{123}Sb.

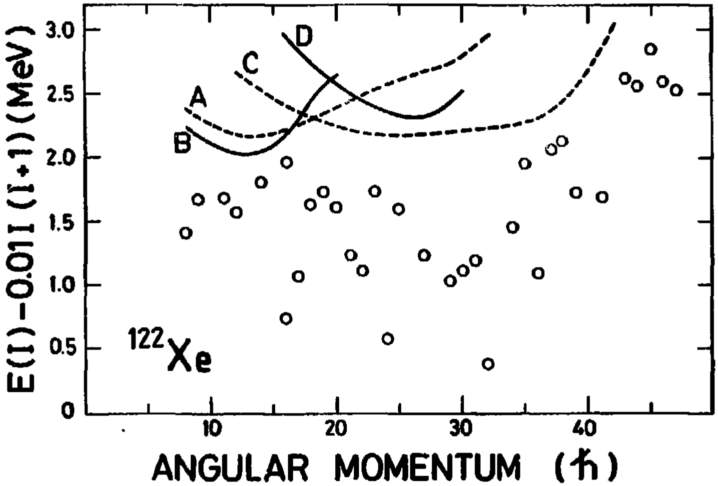

Fig. 11

Energy versus angular momentum calculated by microscopic theory for bands of ^{122}Xe. An average liquid drop contribution of 0.01I(I+1) MeV has been subtracted. Dots indicate the position of yrast non-collective states, whereas the lines indicate the bands listed in table 2. The triaxial bands are found to have almost the same energy as the prolate bands and a $\mathcal{J}^{(2)}_{band} < 30\ \hbar^2/\mathrm{MeV}$ which is apparent as a larger curvature. With a slightly different single-particle potential the triaxial bands could well be yrast. $\mathcal{J}^{(2)}_{band}$ would not be affected by this change.

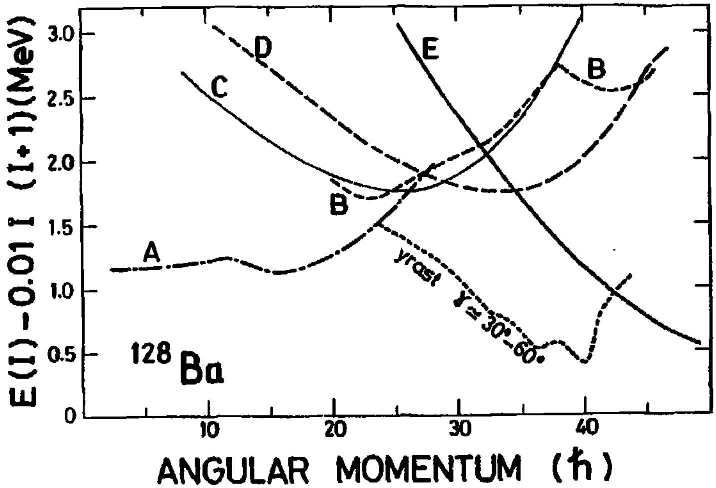

Fig. 12

Energy versus angular momentum as in fig. 11, for bands in ^{128}Ba, which suggests likely cascade and feeding patterns following a heavy-ion reaction. Labels A-E identify the same bands as in table 2. At high spins, highly collective bands like E are most probably populated. Cascades could proceed along such bands well below the spin where E crosses the yrast line, contributing strongly to the $E_\gamma - E_\gamma$ correlations. The fact that discrete transitions are hard to resolve experimentally for $I > 20$ can be explained partly by this mechanism, partly by the high level density in the near yrast region at $I < 30$ and partly by the occurence of additional, less collective, states which are obtained as yrast in this spin region.